Polymer 50 (2009) 1034–1045

Contents lists available at ScienceDirect

Polymer

journal homepage: www.elsevier.com/locate/polymer

Influence of crystal morphology of 1*H*-1,2,4-triazole on anhydrous state proton conductivity of sulfonated bisphenol A polyetherimide based polyelectrolytes

Soma Guhathakurta, Kyonsuku Min*

Department of Polymer Engineering, The University of Akron, Akron, OH 44325-0301, USA

ARTICLE INFO

Article history:
Received 26 August 2008
Received in revised form
17 December 2008
Accepted 19 December 2008
Available online 25 December 2008

Keywords:
Anhydrous proton conductivity
Sulfonated polyetherimide
1*H*-1,2,4-Triazole

ABSTRACT

In this study, new anhydrous proton conducting polyelectrolytes were prepared based on sulfonated bisphenol A polyetherimide (SPEI) and 1*H*-1,2,4-triazole (Taz) as a solid state proton solvent. The effect of degree of sulfonation and triazole concentration on size, shape and dispersibility (crystal morphology) of triazole crystals in sulfonated polyetherimide were examined and correlated with proton conduction. At a constant triazole weight percent, increased sulfonation level caused enhanced nucleation density, reduction of crystallite size and their uniform distribution throughout SPEI matrix. The decrease in size was responsible for the depression of triazole melting temperature. Proton conduction through structure diffusion occurred effectively within the smaller size crystals due to the improved molecular mobility.

1. Introduction

Anhydrous state proton conduction in sulfonated polymers is an important issue in recent years due to the several problems associated with the hydrated systems: evaporation of water and consequently drastic decrease in conductivity, loss of mechanical strength of the membranes due to excessive swelling in water [1–3]. These practical difficulties have stimulated different approaches to develop alternative proton conducting polymer electrolytes. Among various approaches, phosphoric acid doped in basic polymer matrix such as polybenzimidazole showed encouraging results [4–6]. The high proton conductivity observed in the PBI–phosphoric acid complexes originated from the large concentration of intrinsic charge carriers due to the greater extent of self-dissociation of the oxo-acid (it has more donor than the acceptor sites) in contrast to hydrated systems in which high conductivity arise due to high mobility of charge carriers inspite of their low concentration. Another approach, based on similar acid–base interaction is the substitution of water by heterocycles such as imidazole, benzimidazole, pyrazole as proton solvent in acidic polymer matrix [7–10].

1*H*-1,2,4-Triazole is a promising aromatic heterocycle that can act as proton solvent like water due to its amphoteric (proton donor–acceptor sites) nature, intermolecular hydrogen bond formation and self-dissociation characteristics [9,10]. It is a crystalline solid and has a melting point of ~120 °C and boiling point ~256 °C. It has high proton conductivity only above the melting point owing to its self-dissociation. It is electrochemically more stable than imidazole due to the low electron density. Both triazole and triazolium ions ($pK_{a1} = 2.39$, $pK_{a2} = 9.97$) with lower pK_a compared to imidazole ($pK_{a1} = 7.18$, $pK_{a2} = 14.52$) have better proton donating tendency.

The proton conducting polymer electrolyte membranes are key components in a wide variety of applications such as in fuel cells, batteries, supercapacitors, electrochemical sensors and electrochromic devices. The commercially available perfluorosulfonic acid copolymer, for example Dupont's Nafion has been recognized as the potential matrix material due to the high conductivity, high thermal and chemical stability and good mechanical strength. However, the high price, complicated synthetic procedure, limited operation temperature of about 100 °C and high methanol permeability have motivated in seeking of suitable alternatives. Sulfonated polyimide is another promising candidate. This class of well-known high performance engineering thermoplastics possesses excellent thermal and chemical stability, mechanical strength and good film forming ability [11–15].

The introduction of sulfonic acid groups at the macromolecular main chain backbone can induce specific intermolecular interactions including acid–base interaction, hydrogen bonding, ion–dipole or dipole–dipole interaction. The extent of interactions depends on the concentration of acidic group and the type of

* Corresponding author. Tel.: +1 330 972 6675; fax: +1 330 258 2339.
E-mail address: kmin@uakron.edu (K. Min).

0032-3861/$ – see front matter © 2009 Elsevier Ltd. All rights reserved.
doi:10.1016/j.polymer.2008.12.035

counterion. The specific interactions and its influence on ionic conductivity have been reported in few previous studies. Kerres et al. introduced novel acid–base polymer blends that contain network of ionic cross-links (polysalt) formed by proton transfer from polymer acid to polymeric base [16–19]. Examples include sulfonated polysulfone (SPSU), sulfonated polyether sulfone (SPES), sulfonated poly(etheretherketone) as the acidic compound and PSU diaminated at the ortho position to the sulfone bridge, poly(4-vinylpyridine), poly(benzimidazole) (PBI), poly(ethyleneimine) PEI as the basic compounds. Diemede et al. studied the phase separation behavior of polybenzimidazole(PBI)/sulfonated polysulfone(SPSF) blends [20] caused by acid–base interaction. In hydrated system, the sulfonic acid binding sites in polymer also strongly influence its extent of interaction with water and modify the phase transitions of bulk water [21,22]. The state of water in sulfonated polymers rather than the total mass plays more significant role in determining membrane transport properties.

The phase separation behavior of sulfonated polymers is one of the most important factors in controlling the proton conductivity. However, the morphology induced by phase separation is affected by various factors such as different states of hydration [23,24], specific intermolecular interactions [25], casting solvents [26], processing conditions of the membrane [27], hydrothermal history [23,28], etc. Most studies were focused on morphology investigation of hydrated Nafion film using small angle X-ray scattering (SAXS) and scanning probe microscopy (SPM) [29]. Kreuer et al. reported the microstructure of Nafion compared to sulfonated polyarylene [1,30,31]. The hydrophobic/hydrophilic nanophase separation observed in Nafion is not prominent in arylene polymers due to less hydrophobicity of the aromatic backbone, lower acidity of sulfonic acid groups and enhanced rigidity of the main chain.

1*H*-1,2,4-Triazole was used as solid state proton solvent in replacement of water in different polymer matrices such as sulfonated polysulfone and hybrid inorganic–organic polymer network [9], Nafion [32], poly(vinyl phosphonic acid) and poly(2-acrylamido-2-methyl-1-propane sulfonic acid) [33]. To date, no literature is available about the crystal morphology of a heterocycle in sulfonated polymer. In this paper, research is presented to describe the influence of crystal morphology (size, shape and state of dispersion) of 1,2,4-triazole in sulfonated bisphenol A polyetherimide (SPEI) matrix on anhydrous state proton conductivity of the solid polymer electrolyte. The miscibility of SPEI with triazole was investigated as a function of degree of sulfonation and polyelectrolyte composition. The specific intermolecular interactions between SPEI and triazole were characterized by Fourier transform infrared (FT-IR), ^{1}H nuclear magnetic resonance (NMR) spectroscopy and differential scanning calorimetry (DSC). The crystal morphology was studied by wide angle X-ray diffraction (WAXD) technique. Atomic force microscopy (AFM) was used for direct spatial mapping of surface topography and heterogeneity in the polyelectrolyte films. WAXD and AFM were utilized complementarily to interprete the results.

2. Experimental

2.1. Materials

Polyetherimide (ULTEM 1000) was supplied by GE Plastics and dried at 130 °C for 8–9 h under vacuum. Trimethylsilylchlorosulfonate (TMSCS) and 1*H*-1,2,4-triazole (Taz) were purchased from Aldrich Chemical Co. Methylene chloride was dried over molecular sieves prior to its use as sulfonation reaction medium. Dimethylacetamide (DMAc) was used without further purification.

2.2. Procedure

2.2.1. Sulfonation of bisphenol A polyetherimide

Bisphenol A polyetherimide (PEI) was sulfonated using trimethylsilylchlorosulfonate (TMSCS) as sulfonating agent. The detail procedure was described elsewhere [34,35]. To a 250 mL, 3-necked, round-bottomed flask fitted with a condenser, dropping funnel and nitrogen sparge tube, 5 grams of dried polymer was dissolved in 25 mL methylene chloride (~20% w/v solution). The solution was purged with nitrogen for 1 h and TMSCS diluted in 10 mL DCM was added slowly from a dropping funnel. The solution was stirred vigorously at ~30 °C. The reaction mixture after the desired time was precipitated in acetone. The fibrous precipitate was filtered, washed with acetone and dried under vacuum for 24 h. Different degrees of sulfonation were achieved by varying the mole ratio of the sulfonating agent to the PEI repeat unit and the reaction time. Sulfonated polyetherimides were designated as SPEI(*X*)H, where *X* refers to degree of sulfonation.

2.2.2. Preparation of anhydrous proton conducting polyelectrolytes

Anhydrous proton conducting polyelectrolytes were prepared by solution blending of SPEI and 1*H*-1,2,4-triazole (Taz) (5% w/v) in dimethylacetamide (DMAc) at the desired ratio. The solutions were stirred for 2 h and the films were casted on a glass substrate followed by drying at 70 °C till the solvent evaporated. The films were dried under vacuum for 48 h at room temperature. Homogeneous films were obtained. The sulfonated polyetherimides in the acidic form, with three different sulfonation levels 22, 48 and 62% were used to prepare the blends. The polyelectrolytes compositions are described in Table 1.

2.3. Characterization

The sulfonated polyetherimides were characterized by ^{1}H nuclear magnetic resonance (NMR) and Fourier transform infrared (FT-IR) spectroscopy. The degree of sulfonation of sulfonated polyetherimide was quantified by ^{1}H NMR spectroscopy, recorded by Varian 300 MHz. All spectra were obtained from ~3% (w/v) DMSO-d_6 solution at room temperature. Fourier transform infrared spectroscopy of the fibrous sulfonated polyetherimide samples was recorded in attenuated total reflection (ATR) mode using Nicolet 380 FT-IR.

The interactions between SPEI and triazole were characterized by FT-IR (ATR mode) and differential scanning calorimetry (DSC). The sample specimens of proton conducting blends for FT-IR analysis were prepared by casting thin films from 5% (w/v) DMAc

Table 1
Compositions of SPEI(*X*)H/triazole polyelectrolytes.

Sample designation	Degree of sulfonation (DS) (%)	Triazole content (wt%)	λ[a]
SPEI(22)H/Taz 100/0	22	0	0
SPEI(22)H/Taz 90/10	22	10	3
SPEI(22)H/Taz 70/30	22	30	13
SPEI(22)H/Taz 50/50	22	50	31
SPEI(48)H/Taz 100/0	48	0	0
SPEI(48)H/Taz 90/10	48	10	2
SPEI(48)H/Taz 70/30	48	30	6
SPEI(48)H/Taz 50/50	48	50	15
SPEI(62)H/Taz 100/0	62	0	0
SPEI(62)H/Taz 90/10	62	10	1
SPEI(62)H/Taz 70/30	62	30	5
SPEI(62)H/Taz 60/40	62	40	8
SPEI(62)H/Taz 50/50	62	50	12

[a] λ is defined as number of moles of triazole per mole of sulfonic acid group.

solution followed by drying at 70 °C till the solvent evaporated at room temperature under vacuum for 24 h. FT-IR spectra of the samples were scanned in the absorbance mode from 4000 to 400 cm^{-1} with 32 scans and a resolution of 4 cm^{-1}. The acid–base complex formation between SPEI and triazole molecules was analyzed by ^1H NMR in DMSO-d_6.

The melting temperatures of triazole in the polyelectrolytes were determined by TA 2920 Differential scanning calorimeter (DSC). The samples were heated from room temperature to 140 °C at a heating rate of 10 °C/min. All experiments were performed with 10–12 mg sample, sealed in aluminium hermetic pans under nitrogen atmosphere.

In addition to the above mentioned techniques, the crystal morphology of triazole in the SPEI(*X*)H was characterized by wide angle X-ray diffraction (WAXD). WAXD film patterns were obtained by using Bruker AXS D8. X-ray was monochromatized with a nickel foil filter ($\lambda_{Cu\ K\alpha} = 1.54$ Å). The generator was operated at 40 kV and 40 mA. The sample to film distance was kept constant at 15 cm for all samples.

The surface morphologies of the polyelectrolyte films were investigated by atomic force microscopy (AFM) using Multi Mode Scanning Probe Microscope model with a Nanoscope IIIa Controller. The samples were prepared by mixing the desired weight fractions of SPEI and triazole in dimethylacetamide solutions. Thin films were obtained by casting the solutions on puck. The solvent was slowly evaporated at 60 °C and then at room temperature in a vacuum oven for 24 h. The atomic force microscope was operated in tapping mode using silicon cantilever probes with the spring constant ranging between 20 and 80 N m^{-1}. The resonance frequency of the oscillating probe was in the range of 250–300 kHz. The topography and phase images were recorded simultaneously under ambient conditions with a scan rate of ~1 Hz for 5 μm scan size, and ~2 Hz for 0.5–1 μm scan size with constant integral and proportional gain for all samples. Scanning was performed at different locations of each sample to ensure the reproducibility of the images.

2.4. Measurement of proton conductivity

The proton conductivity was determined by impedance measurement using alternating current method. The polymer film was sandwiched between two stainless steel electrodes in a two terminal method. In the frequency range 100 Hz to 100 kHz, Hewlett Packard 4274A impedance analyzer was used to obtain the magnitude of impedance, $|Z|$ and the phase angle, θ. The bulk resistance of the film was taken as the value of Z' (real axis) which produced the minimum imaginary response (Z''). The resistance was converted to specific conductivity, σ (unit Siemens/cm) by the following equation:

$$\sigma = l/R_b A \tag{1}$$

where l is the distance between the electrodes and A is the film surface area perpendicular to the flow direction. The temperature dependence of proton conductivity was studied by attaching the whole assembly with a heating device and using a heating rate of 10 °C/min.

3. Results and discussion

3.1. Analysis of intermolecular interactions between immobilized sulfonic acid groups and triazole molecules

3.1.1. Spectroscopic analysis

In FT-IR spectra of triazole (not shown), the doublets at 1270, 1260 cm^{-1} and 1180,1144 cm^{-1} were assigned to C–N asymmetric and symmetric stretching and the absorption bands at 1060 and 1020 cm^{-1} were attributed to N–N asymmetric and symmetric stretching respectively. The bands at 978, 955, 881 and 669 cm^{-1} were associated with the ring deformation and ring torsion [36–38].

The activated bisphenol A moiety of polyetherimide was sulfonated to various levels as evident from ^1H NMR spectra in Fig. 1. The spectra shows appearance of singlet at 7.79 ppm (e) corresponding to the protons adjacent to the sulfonic acid group and two doublets at 6.98 (i, j) and 7.88 ppm (f, g) associated with the sulfonated bisphenol A unit. The degree of sulfonation (DS) was quantified by ^1H NMR in DMSO-d_6. The quantification is based on the chemical structure of SPEI, there are 18 aromatic protons in the non-sulfonated repeat unit and 16 aromatic protons in the sulfonated repeat unit with one proton adjacent to sulfonic acid group at 7.79 ppm. Since this peak is well resolved from all other peaks, it has been used for quantification purpose. The degree of sulfonation is given by,

$$\mathrm{DS} = \frac{18R}{1+2R},\ R = \frac{A_e}{A} \tag{2}$$

R is defined as the ratio of the area under the peak at 7.79 ppm, A_e, to the sum of the area under the peaks corresponding to all other aromatic protons, A.

FT-IR spectra of SPEI at different sulfonated levels are shown in Fig. 2. In sulfonated polyarylene ethers, the absorption band at 1010 cm^{-1} is assigned to the symmetric stretching of the diphenylether unit along the polyarylene ether main chain and in plane ring vibration of *para*-substituted aryl ether. The bands at 1028, 1090 and 1170 cm^{-1} were assigned to the symmetric and asymmetric stretching of the sulfonate group [20,39]. In the present study, with acid form of sulfonated polyetherimide, extensive hydrogen bond formation resulted broad absorption bands at 1020 and 1160 cm^{-1} due to symmetric and asymmetric stretching of sulfonic acid group with a relatively sharp peak at 1090 cm^{-1}, associated with free sulfonic acid groups. The absorption peak at 1360 cm^{-1} attributed to symmetric bending deformation of methyl groups in isopropylidene units is insensitive to the sulfonation and was used as internal standard. All spectra were normalized with respect to this band since the intensity was same in all cases. The spectral changes observed with increased sulfonation level, as depicted in Fig. 2 are as follows: (i) intensity of the peak at 1090 cm^{-1} increases, (ii) the absorption bands at 1010 and 1160 cm^{-1} gradually broaden.

Based on the FT-IR spectra of the individual components, the spectral regions at 650–1000 and 800–1300 cm^{-1} are focused to analyze the specific intermolecular interactions between SPEI(*X*)H and triazole as a function of sulfonation level and triazole concentration. The characteristic bands involved in the intermolecular interactions are summarized in Table 2.

The effect of degree of sulfonation and triazole concentration on the absorption bands of triazole in SPEI(*X*)H/Taz can be summarized as follows: (i) the absorption peaks at 669 881 954 and 978 cm^{-1} broaden and exhibit red shift with increasing sulfonation level in 70/30 compositions compared to neat triazole (Fig. 3a). The shift is very clear in SPEI(22)H/Taz beyond which it becomes insignificant while the peak area increases with degree of sulfonation, particularly at 881 and 978 cm^{-1}. The peaks are relatively sharp in 50/50 composition and show slight blue shift (Fig. 3b), (ii) a new peak appears at 972 cm^{-1} at 62% sulfonation level in SPEI(62)H/Taz 50/50 composition, (iii) The C–H deformation, C–N and N–N stretching peaks at 1144, 1260 and 1060 cm^{-1} also exhibit slight blue shift with increasing sulfonic acid content, the effect is more prominent in 50/50 composition as shown in Fig. 3b.

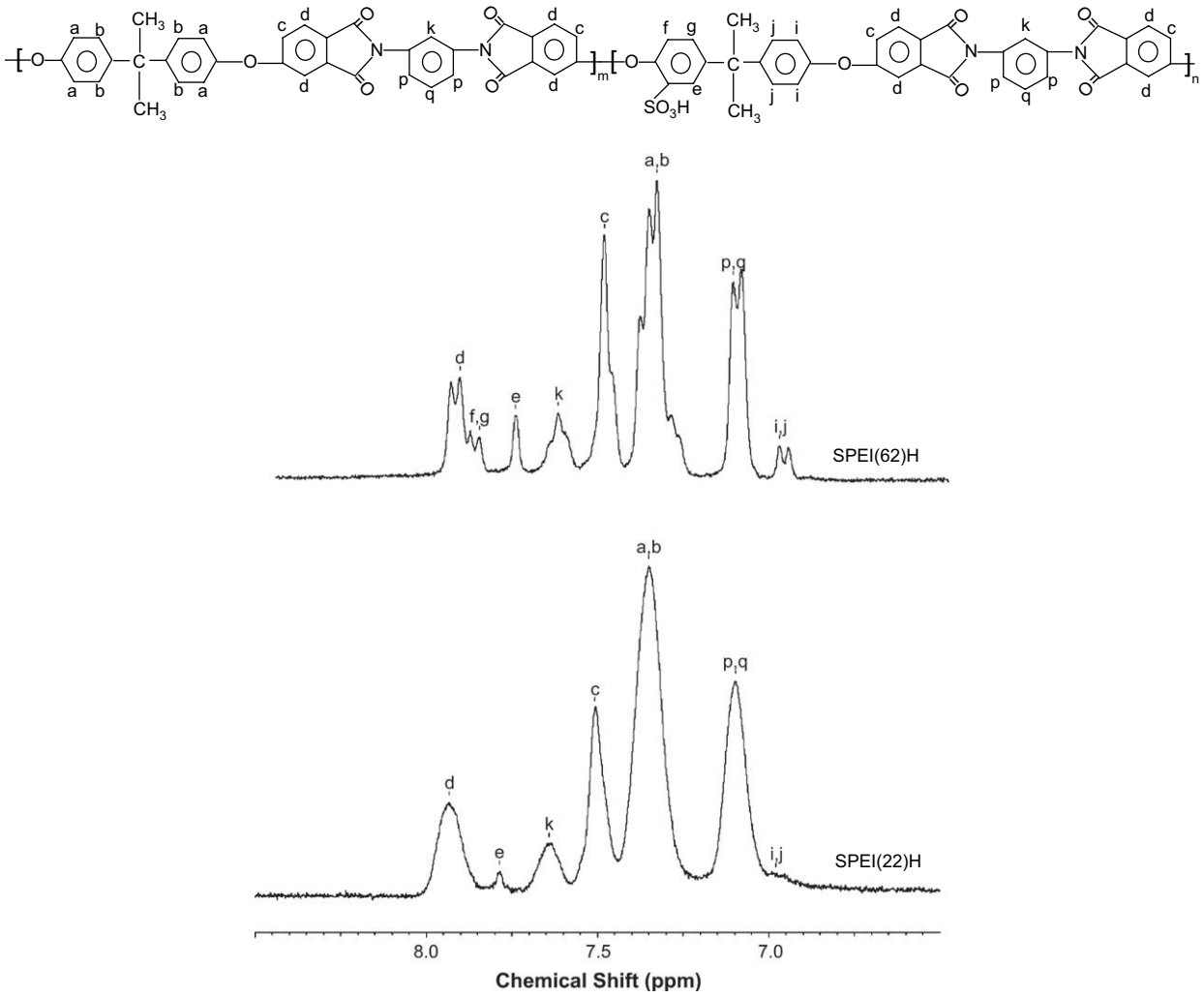

Fig. 1. [1]H NMR of SPEI sulfonated by trimethylsilylchlorosulfonate (numbers refer to degree of sulfonation).

It is well known that in pure triazole, molecules are in self-association through N–H···N and C–H···N intermolecular hydrogen bonding [40]. In sulfonated polyetherimide matrix, triazole formed hydrogen bonds mainly with sulfonic acid groups thus with increasing sulfonation level the interactions between triazole molecules with sulfonated polyetherimide became predominant. This caused red shift of the bands characterizing triazole ring deformation and ring torsion. At a given triazole weight percent, e.g. 70/30 composition, certain amount of triazole molecules involved in strong interaction with sulfonic acid groups causing red shift, remaining are weakly bound and/self-associated triazole. The strength of interactions in decreasing order is: triazolium ion–sulfonate anion > triazole–sulfonate > triazole–sulfonic acid ≈ triazole–triazole > triazole–hydrophobic polyetherimide backbone. The bands associated with strongly and weakly bound triazole overlapped in most cases exhibiting peak broadening except in SPEI(62)H/Taz 50/50 composition where the strongly

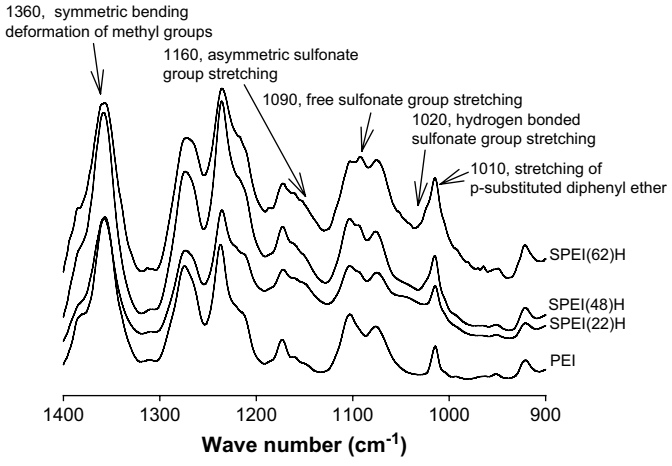

Fig. 2. FT-IR spectra of SPEI at various sulfonation levels (numbers refer to degree of sulfonation).

Table 2
FT-IR absorption bands of SPEI and 1*H*-1,2,4-triazole involved in intermolecular interactions.

Components	Wave number (cm^{-1})	Assignment
Triazole	669	Ring torsion
Triazole	978,954,881	Ring deformation
Triazole	1060	N–N asymmetric stretching
Triazole	1144	C–H deformation/C–N symmetric stretching
Triazole	1260	C–N asymmetric stretching
SPEI	1090	Symmetric stretching of sulfonic acid group

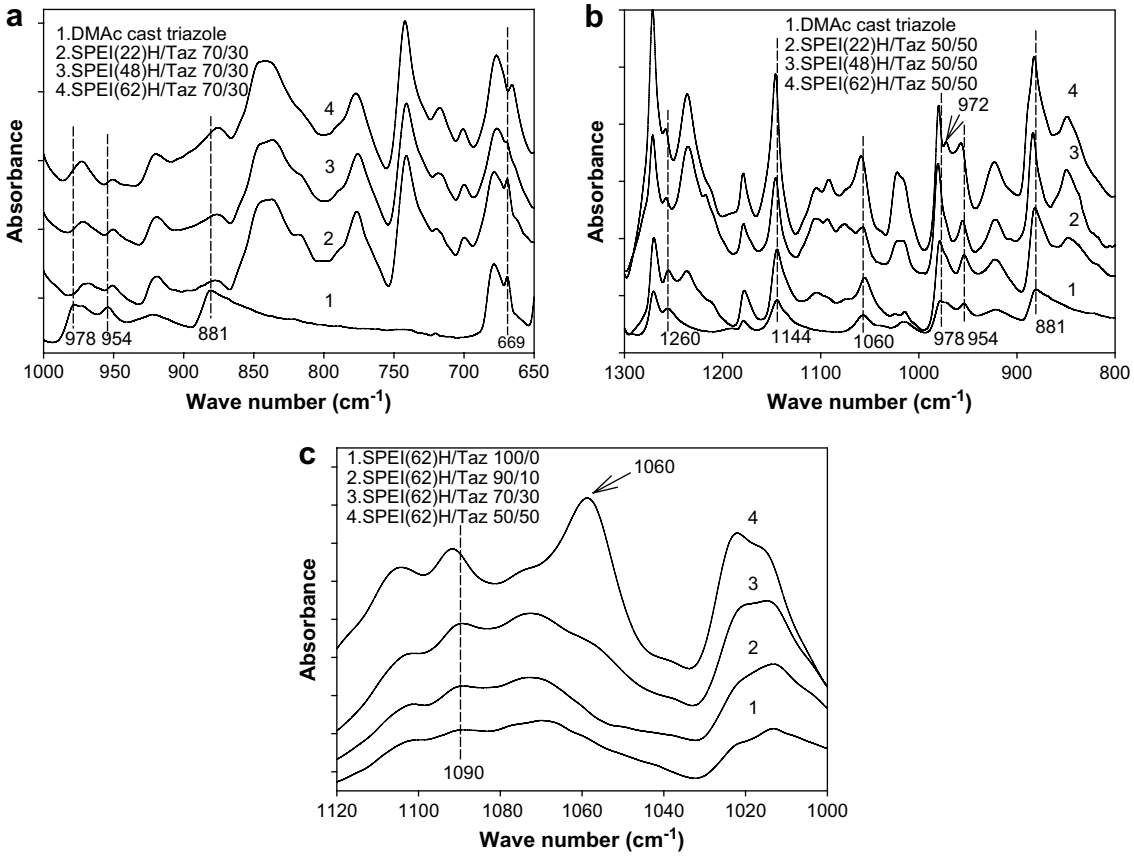

Fig. 3. a) Effect of degree of sulfonation on ring torsion of triazole (650–1000 cm^{-1} region) in 70/30 compositions, b) Effect of degree of sulfonation on triazole characteristics bands (800–1300 cm^{-1} region) in 50/50 compositions, c) Effect of triazole concentration on symmetric stretching band of sulfonic acid group.

bound triazole appeared as a new peak at 972 cm^{-1} in Fig. 3b. At a constant triazole concentration, with increasing degree of sulfonation, the amount of triazole involved in the interaction with sulfonic acid groups increased thus increasing peak area rather than peak maxima. In 50/50 composition, weakly bound/self-associated triazole molecules predominated and the slight blue shifts observed for the triazole characteristic bands were due to the weakening of N···H–N and C–H···N hydrogen bonding between triazole molecules, the extent of which increased with sulfonation level. The similar behavior was observed in PBI/SPSU and PBI/poly(vinyl-acetate-stat-vinyl alcohol) blends where the blue shift of N–H stretch was described as weakening of self-association in PBI [20,41].

In sulfonated polymers, the symmetric stretching band of sulfonic acid group is very sensitive to local environments and has been used to study the interactions in polymer blends [20,22]. In the present study on SPEI(*X*)/Taz system, the absorption band at 1090 cm^{-1} assigned to symmetric stretching of free sulfonic acid groups was used to monitor the specific interactions with triazole as there is no absorption band of triazole in the spectral region. As illustrated in Fig. 3c, the peak shows a clear shift to higher wave number with increasing triazole concentration and becomes more pronounced in 50/50 composition at 62% sulfonation level. The addition of triazole molecules in SPEI matrix caused protonation of nitrogen atom in heterocyclic ring. The sulfonic acid groups of SPEI formed hydrogen bonds with triazole molecules and the strength of the hydrogen bonds differ from hydrogen bonding interaction between self-associated triazole molecules. As the number of triazole molecules interacting with sulfonic acid site of SPEI increased, the peak shifted to higher wave number. The same trend was also observed in Nafion/polypyrrole composites, the symmetric stretching peak of sulfonate group shifted to higher frequency with increasing polypyrrole content [25].

3.1.2. DSC

Fig. 4 describes the effect of degree of sulfonation on the melting endotherm of triazole. It is apparent that increased specific interactions between triazole molecules and sulfonated polyetherimide

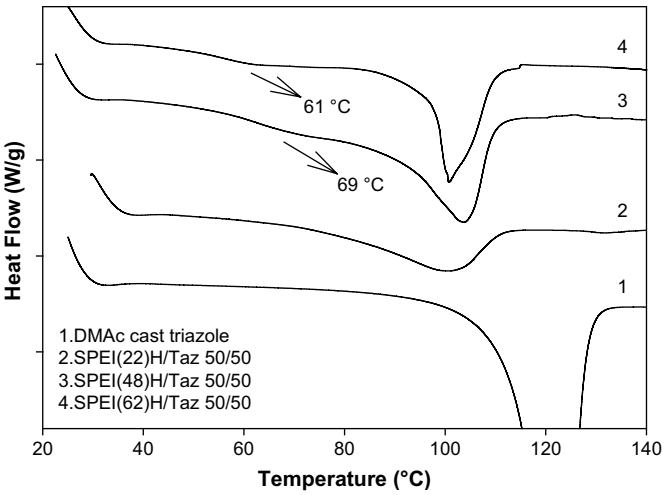

Fig. 4. Effect of degree of sulfonation on melting temperature of triazole in 50/50 compositions.

with increasing sulfonation level cause depression of melting temperature. The effect of triazole concentration on its melting temperature and enthalpy of fusion at three different sulfonation levels is illustrated in Fig. 5. The melting peak and enthalpy gradually shifted to higher value with increasing triazole concentration.

Triazole molecules crystallized in sulfonated polyetherimide matrix were mainly in two different states: (i) triazole strongly bound to the sulfonic acid sites; (ii) weakly bound triazole i.e., molecules weakly bound to the specific binding sites in the polymer or to the strongly bound triazole and/or free triazole, triazole that behaves like bulk triazole. At a given sulfonation level, a certain portion of triazole molecules were strongly bound to the sulfonic acid groups and the remaining were weakly bound/free triazole. With increasing triazole content, the weakly bound triazole concentration increased causing the melting endotherm shift to higher temperature. Fig. 4 (curves 3 and 4) also shows two endotherms consisting of the broad melting peaks from 60 to 70 °C, assigned to the strongly associated triazole and a relatively sharp peak at 100–105 °C due to the weakly associated triazole at higher triazole content (50 wt%) in SPEI(48)H/Taz and SPEI(62)H/Taz. The splitting of the absorption bands due to the strongly and weekly bound triazole molecules was also observed in the FT-IR spectra for SPEI(62)H/Taz (Fig. 3b). It is difficult to quantify each state of triazole by DSC due to numerous contributing factors: (1) overlapping of melting endotherms, (2) enthalpy of fusion is a function of the strength of interaction (3) the change in heat capacity associated with the highly dispersed triazole or the concentration of triazole (e.g. in 90/10 composition) is too small and beyond the detection limit of the technique.

3.2. NMR study on the protonation of triazole by sulfonic acid

NMR titration has been widely used to estimate the extent of proton transfer from a dopant acid to the model heterocyclic compound [8,42,43]. Schuster et al. determined the protonation constants of imidazole by trifluoroacetic acid and acetic acid [8]. The equilibrium constant using trifluoroacetic acid as dopant was between 60 and 160 depending on temperature. The protonation of triazole by sulfonic acid group of SPEI(62)H was examined from the chemical shift (∂_{obs}) of C(5)H of triazole ring at 8.28 ppm by ^{1}H NMR spectra since SPEI has no peak in the region (Fig. 6a). ∂_{obs} Shifted to higher value at high acid concentration ($\geq$56 wt%). No significant change of chemical shift was observed at low acid concentration (Fig. 6b). Our effort to find the protonation constant of triazole by sulfonic acid was not successful probably due to the weaker acidic nature since the acidic group is located at the activated bisphenol A unit of poly(arylene ether). The chemical shift change with acid concentration provided qualitative explanation of acid–base complex formation.

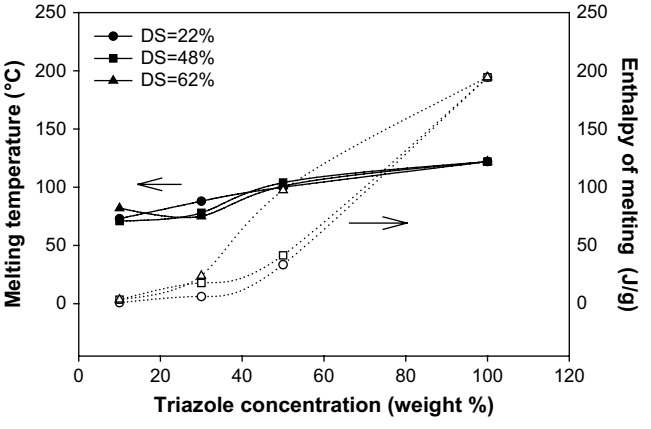

Fig. 5. Melting temperature and enthalpy of fusion as a function of triazole content at various sulfonation levels.

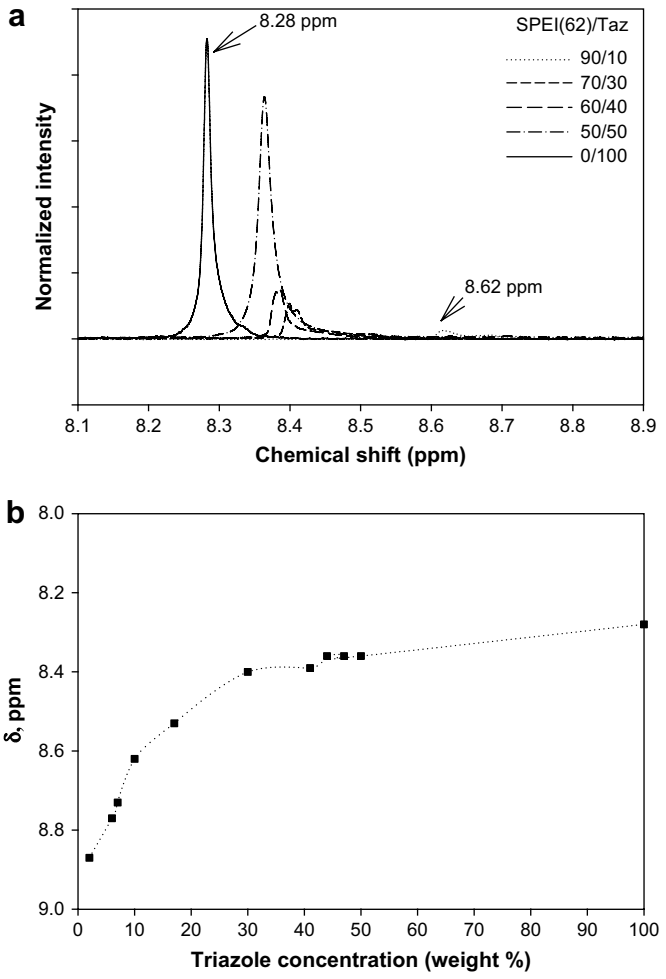

Fig. 6. a) ^{1}H NMR spectra of chemical shift of triazole (C(5)H) in SPEI(62)H matrix. b) Proton chemical shift (C(5)H of triazole) as a function of triazole concentration.

3.3. Crystal morphology of triazole dispersed in sulfonated polyetherimide

3.3.1. WAXD analysis

The room temperature crystal structure of 1,2,4-triazole was first determined by Deuschl [44]. 1*H*-1,2,4-Triazole is orthorhombic, space group symmetry *Pbca* and unit cell parameters calculated as $a = 9.69 \pm 0.04$ Å, $b = 9.38 \pm 0.04$ Å and $c = 7.14 \pm 0.03$ Å with eight molecules in the unit cell. Triazole exists in two tautomeric forms. The nitrogen-bonded hydrogen atom could not be located in the room temperature X-ray diffraction study. Thus the crystal structure was further investigated by Goldstein et al. at a low temperature about −160 °C [40]. The tautomeric hydrogen was found to be in 1st position. The triazole ring is planar, the molecules are linked together through N–H···N and C–H···N hydrogen bonds and form corrugated sheet structure. Comparison of X-ray diffraction patterns of solution cast triazole with triazole crystallized in SPEI(*X*)H at different sulfonation levels shows a sequence of spots for dimethylacetamide cast triazole, these spots gradually lie on Debye–Scherrer rings and finally produces smooth, continuous

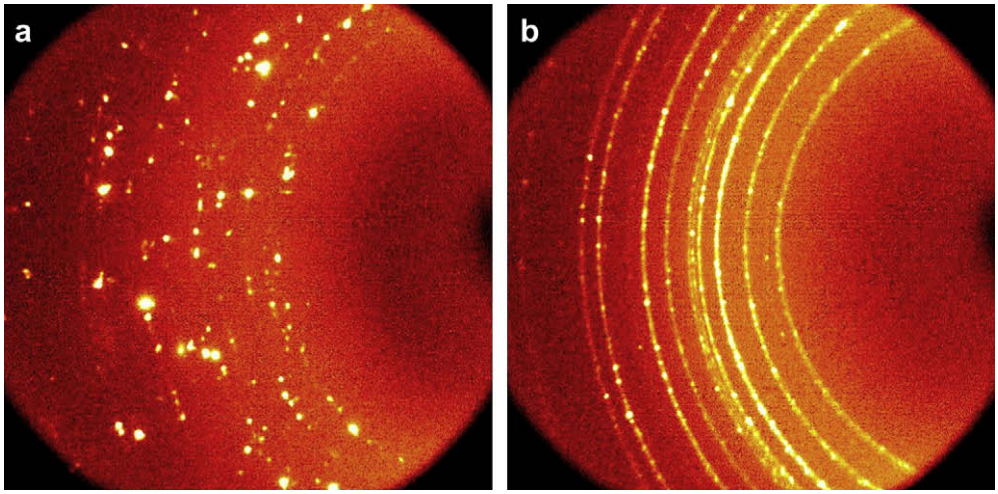

Fig. 7. WAXD patterns of (a) DMAc solution cast triazole crystals, (b) SPEI(62)H/Taz 60/40.

rings with increasing sulfonation level depending on triazole concentration, two examples are depicted in Fig. 7.

In Fig. 8a, WAXD diffractograms at 2θ about 17.7° corresponding to (111) lattice planes of triazole in SPEI(*X*)H at different degrees of sulfonation are compared with that of pure solution cast triazole. From the peak position and peak width, the apparent lateral crystal size, L_{hkl} or size in the direction perpendicular to the reflection plane, *hkl* was calculated using Scherrer equation [45]:

$$L_{hkl} = \frac{0.9\lambda}{\beta_{hkl}\cos\theta} \tag{3}$$

Where λ is the wave length of X-ray, β_{hkl} is the crystal reflection width (in radian) at half the maximum intensity, θ is the Bragg angle of *hkl* reflection and 0.9 is the value set to the crystal shape factor. The results are summarized in Table 3. It is apparent in Fig. 8a that the peak corresponding to (111) diffraction of triazole in SPEI(*X*)H gradually broadens upon increasing sulfonation level and the peak maxima appears at wider angle compared to that in pure triazole indicating that the lattice planes in triazole crystallites within sulfonated polyetherimide were more closely spaced than in pure triazole. There is little variation in peak maxima value with degree of sulfonation The peak broadening was associated with the reduction in crystal size due to increased interaction with sulfonic acid groups (Table 3). The effect of triazole concentration on (111) diffraction at a given degree of sulfonation (22%) is depicted in Fig. 8b. The peak intensity increases with triazole concentration and the maxima shifted towards that of pure triazole. This clearly indicates existence of two different degrees of interaction between triazole molecules and sulfonic acid groups, also evident from DSC thermograms and FT-IR spectroscopy. The strongly associated triazole molecules in which the lattice planes were closer than in pure triazole and weakly bound triazole. The behavior of loosely bound triazole molecules closely resembles pure triazole.

The sulfonic acid groups provided strong binding sites and induced nucleation of triazole. The crystals grown from pure solution showed spotty pattern owing to their larger size. At constant triazole weight percent, increased sulfonation level caused enhanced nucleation density thus reduction of crystal domain size. Furthermore, the uniform distribution of the acidic groups in the polymer also resulted homogeneous dispersion of triazole crystals throughout the polymer matrix. Larger number of smaller size crystallites covered a broader spectrum of angles in the

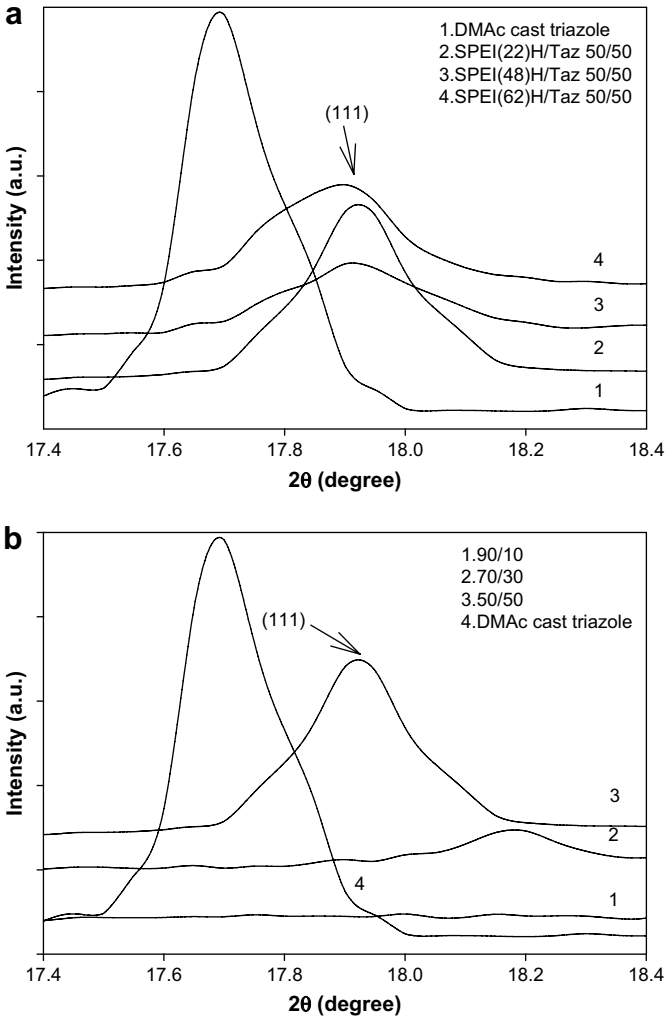

Fig. 8. a) WAXD diffractograms of SPEI(*X*)H/Taz 50/50 at different degrees of sulfonation for (111) plane. The pattern of dimethylacetamide cast triazole is presented as a reference. b) WAXD profiles of SPEI(22)H/Taz at different weight percent of triazole.

Table 3
Comparison of *d* spacing and crystal size measured by WAXD technique.

Degree of sulfonation (DS) (%)	Triazole content (wt%)	2θ (°)	*d* spacing (Å)	$L_{(111)}$ (nm)
0	100	17.75	4.99	44.65
22	30	18.19	4.9	40.21
22	50	17.89	4.96	42.31
48	30	17.78	4.98	23.99
48	50	17.89	4.96	30.34
62	30	18.16	4.9	–
62	40	17.9	4.95	20.61
62	50	17.89	4.96	22.33

azimuthal direction, eventually forming Debye–Scherrer rings. Cullity reported a similar spot to ring pattern formation in metallurgical crystals due to the decrease in grain size [45]. The detection of crystal reflection peaks by WAXD was affected by the triazole concentration and the crystal size. At low triazole concentration (i.e., 10 weight percent) and small crystal size in SPEI(62)H/Taz 70/30, the signals are too weak to be detected by X-ray diffraction. This assertion was further verified by atomic force microscopy.

3.3.2. AFM image analysis

In Fig. 9, three dimensional topographic images of SPEI(*X*)H/Taz 70/30 composition with different sulfonation levels, 22, 48 and 62 are shown. The operational parameters were kept constant for comparison of the images of different samples as described in the Experimental section. In SPEI(*X*)H/Taz film surface, some distinct features are observed, which are not seen in neat SPEI (not shown), hence assigned to the triazole crystal domains. The variation in size, shape and dispersity of the crystal domains of triazole is evident with enhancing sulfonation level. The domains are elevated (brighter in color) at lower sulfonation level (22%), while they are depressed (darker in color) with respect to the surrounding matrix at higher degree of sulfonation. In SPEI(62)H/Taz topographic image, a majority of the domains have relatively circular cross-section with a reduction in size compared to that in SPEI(48)H/Taz, also observed in the images at higher magnification, scan size 500 nm (Fig. 10a and b). Furthermore, the triazole crystallites are uniformly distributed all over the surface at greater sulfonation level and higher resolution topographic image analysis reveals the crystal domains are interconnected (Fig. 10 (c)) with contrast variation in each domain.

The phase images of SPEI(62)H/Taz polyelectrolytes with varying triazole concentration are displayed in Fig. 11. The phase images have crystal domains brighter in color within relatively darker color matrix, the size of the domains increases with increasing triazole weight percent. In 70/30 and 60/40 compositions, the domains also have circular cross-section while with 50 weight percent triazole content, two types of discrete domains are seen, smaller (darker in color) domains are separated from larger (brighter in color) domains. In 90/10 composition, the crystallites have very loose structures due to insufficient triazole content while at higher triazole weight percent, dense domain structures are evident.

The sulfonic acid groups acted as nucleation sites for the triazole crystals. The specific intermolecular interactions between triazole molecules and sulfonic acid groups controlled uniform radial growth and resulted homogeneous dispersion of the crystal domains. With increasing sulfonation level, the increased number of nucleation sites caused reduction of crystal size at a given triazole concentration. The triazole molecules at lower sulfonation level were not intimately bound to polymer chains thus produced roughness. The solvation of triazole by the sulfonated polymer matrix and consequently size reduction caused melting point depression of triazole crystals. The onset of melting of these smaller

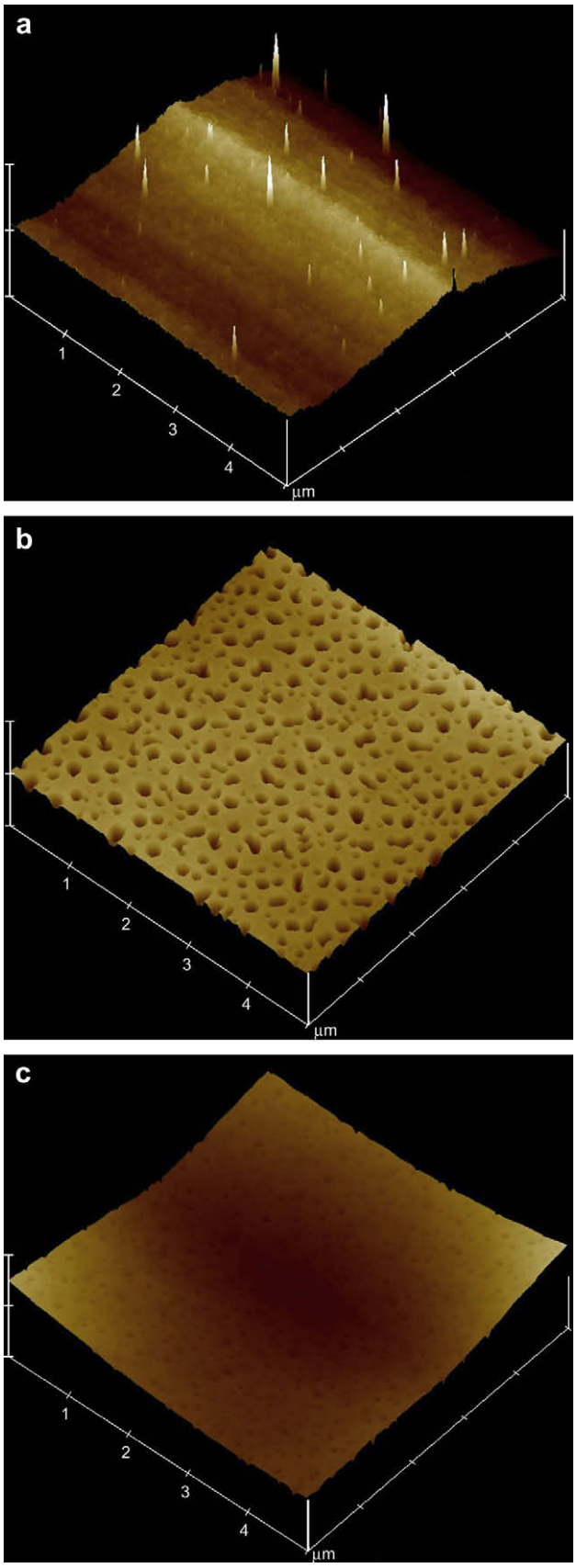

Fig. 9. Tapping mode three dimensional topographic images of SPEI(*X*)H/Taz 70/30 (scan size = 5 µm) at (a) *X* = 22%, (b) *X* = 48%, (c) *X* = 62%.

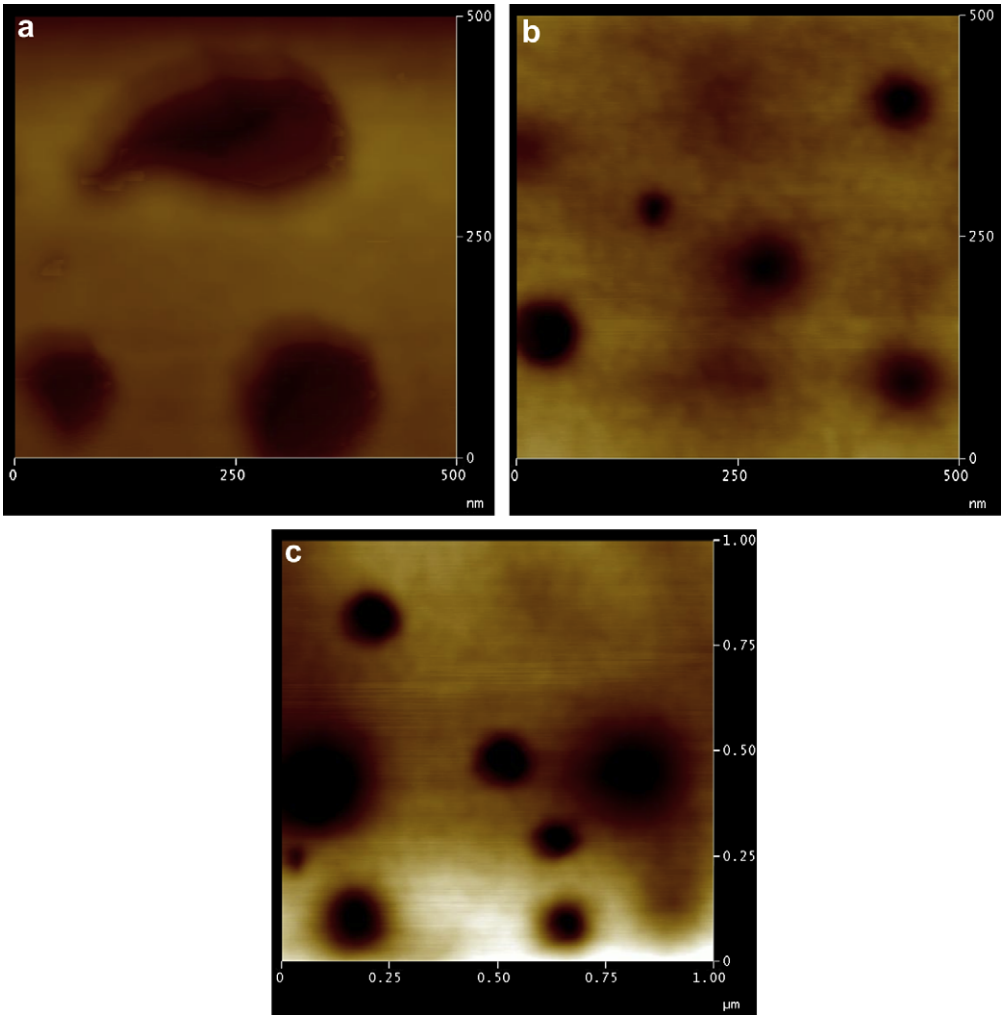

Fig. 10. Height images of SPEI(*X*)H/Taz at higher magnification for (a) $X = 48\%$, 70/30 (scan size = 500 nm), (b) $X = 62\%$, 70/30 (scan size = 500 nm), (c) $X = 62\%$, 60/40 (scan size = 1 μm).

size crystals in SPEI(62)H was close to the room temperature. The softening of crystal domains was probably responsible for the contrast reversal observed in three-dimensional images, the hills collapsed into valleys (Fig. 9). The strongly bound triazole molecules in most of the cases are surrounded by the weakly bound ones, resulting contrast variation in each domain. In SPEI(62)H/Taz 50/50 composition two distinguishable crystal domains observed in AFM phase image resulted two different melting transitions. The similar concept of controlled crystallization of small molecules in host polymer matrices has been exploited in previous studies. Lin et al. found strong binding of cadmium sulfide through ether oxygen atoms of polyethylene oxide (PEO) induce nucleation and resulted crystals of uniform size and morphology [46]. The sulfonic acid induced triazole crystal morphology played significant role in the regulation of proton transport in SPEI/Taz polyelectrolytes.

3.4. Proton conduction

Fig. 12 shows the conductivity data against triazole concentration (weight percent) and also as a function of λ, defined as number of moles of triazole per mole of sulfonic acid group (n_{Taz}/n_{SO3H}) at various degrees of sulfonation. At a given sulfonation level, upon increasing triazole content, conductivity increases up to 30–40 wt% triazole, beyond which it falls. This can be attributed to the fact that above a certain weight percent of triazole content, the behavior of polyelectrolyte matrix approached the properties of bulk triazole. It is also seen that the conductivity increases with degree of sulfonation at a constant triazole weight percent and at constant λ. This behavior can be explained in terms of relative ratio of sulfonic acid bound triazole to free triazole, the increase of which resulted significant rise in conductivity.

The proton conductivity of SPEI(*X*)H/Taz polyelectrolytes exhibited Arrhenius-type temperature dependence, a linear least square fit to the data is shown in Fig. 13. As the glass transition temperature of SPEI is higher than the temperature employed in the study, large scale segmental mobility was hindered, conduction mechanism coupled with solvent dynamics occurred in SPEI(*X*)H/Taz polyelectrolytes.

The anticipated mechanistic pathway of proton conduction as shown in Fig. 14 can be illustrated as follow: Proton conduction in SPEI/Taz polyelectrolytes occurred in the triazole phase and the immobile sulfonic acid groups acted as proton donors. Spectroscopic study revealed acid–base interaction between proton donor and acceptor sites (triazole). WAXD and AFM analysis demonstrated gradual reduction of triazole crystal size and their uniform distribution throughout the polymer matrix with increasing degree of sulfonation. The reduction of size caused melting point depression of triazole. The onset of melting of some of these smaller size crystals was close to room temperature. Thus the molecular mobility of triazole within SPEI(62)H matrix started to contribute

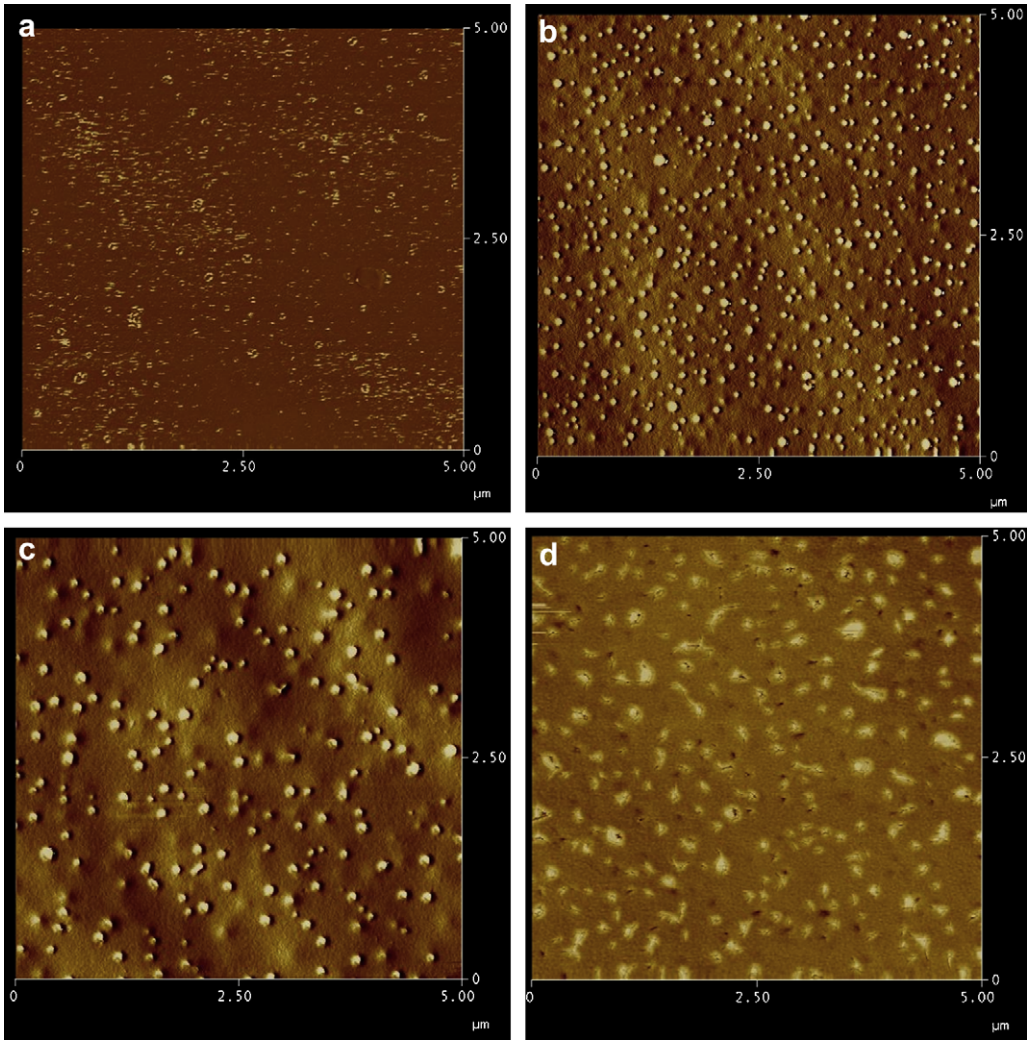

Fig. 11. Phase images of SPEI(62)H/Taz at various triazole concentrations (weight percent) (scan size = 5 μm), (a) 10%, (b) 30%, (c) 40%, (d) 50%.

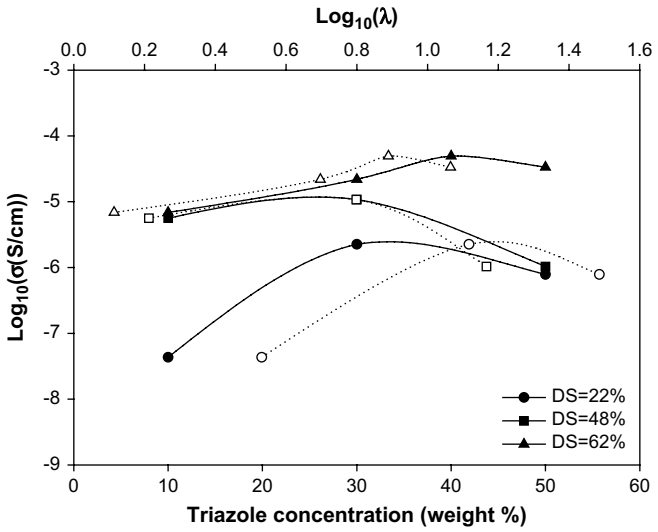

Fig. 12. Proton conductivity at 30 °C in SPEI(*X*)H/Taz polyelectrolytes at various degrees of sulfonation. The filled and open symbols represent conductivity against triazole weight percent and λ respectively.

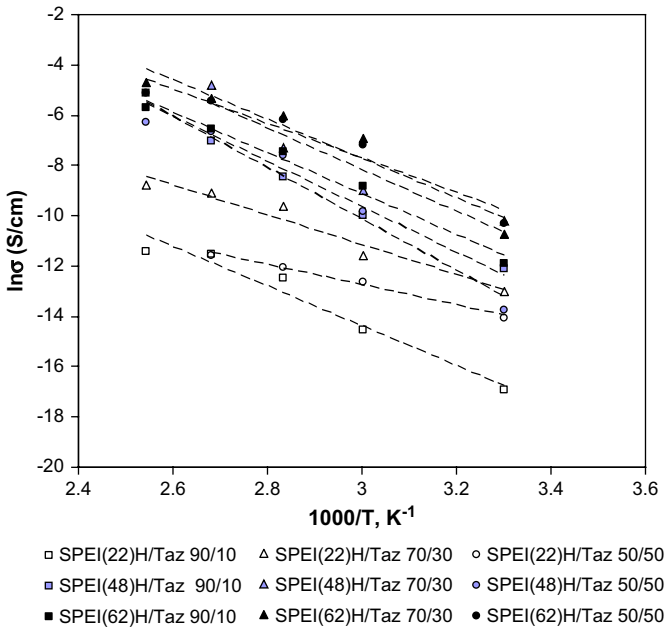

Fig. 13. Temperature dependence proton conductivity of SPEI(*X*)H/Taz polyelectrolytes.

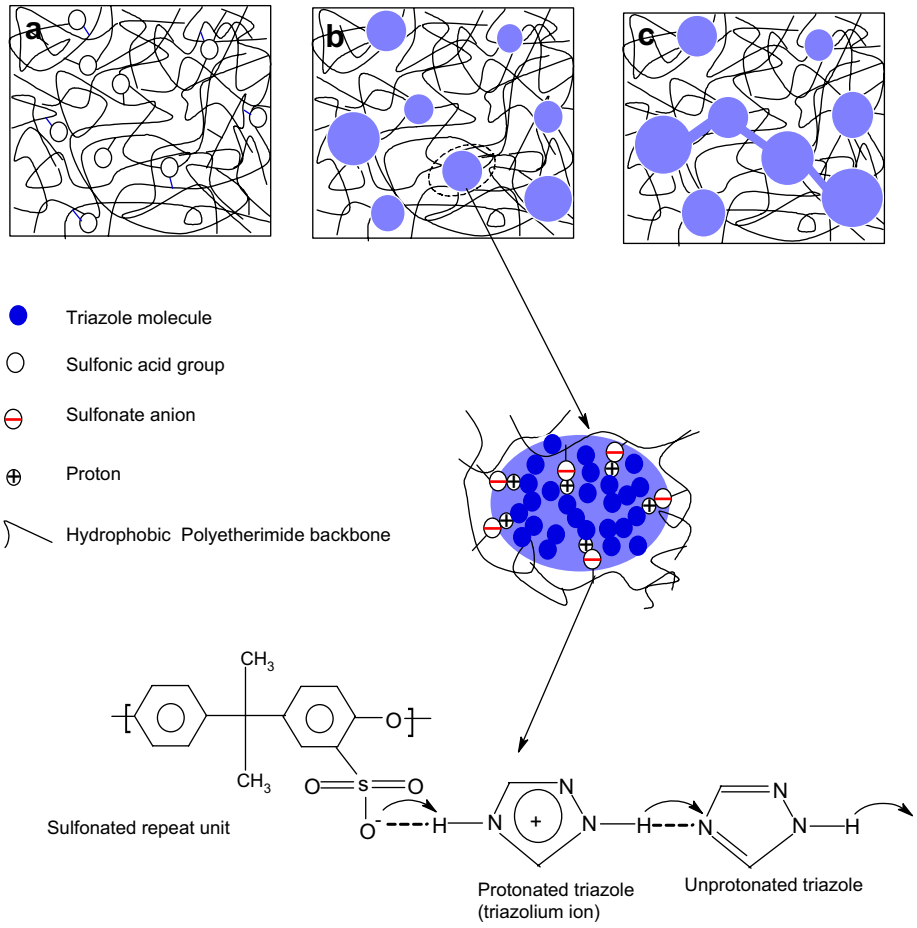

Fig. 14. Schematic representation of morphology evolution of triazole crystals in sulfonated polyetherimide matrix. a) Random distribution of sulfonic acid groups in SPEI, b) Crystallization of triazole at sulfonic acid sites, c) Interconnected triazole crystal domains. Intermolecular proton transfer mechanism between protonated and unprotonated triazoles through hydrogen bonded network in SPEI(*X*)H/1,2,4-triazole matrix(structure diffusion) shown by the arrow.

far below the melting temperature of pure triazole. Different degrees of association of triazole molecules to the sulfonic acid sites were evident from FT-IR and DSC results. Within each crystal domain, certain fraction of triazole molecules was strongly associated with the sulfonic acid binding sites, remaining were weakly bound or self-associated free triazole. The excess protons originating from the immobile sulfonic acid groups caused protonation of the triazole ring (triazolium ion formation). The neutral and protonated triazole molecules formed hydrogen bonded network or structure similar to that in hydrated acidic polymers [1,2] and intermolecular proton transfer within the hydrogen bonded network occurred through hydrogen bond breaking and formation (structure diffusion, shown by arrow in Fig. 14). With increasing sulfonation level, the concentration of triazolium ions increased. Comparing the 70/30 composition of SPEI(62)H/Taz and SPEI(22)H/Taz, conductivity in the former is higher by a factor of about 10 at 30 °C indicating the function of triazolium ions as a source of charge carriers. The proton self-diffusion coefficient in 1*H*-1,2,4-triazole/$C_{12}PhSO_3H$ with 9 mol% acid was 2.0×10^{-10} m^2/s which was one-fourth of the conductivity diffusion coefficient (7.2×10^{-10} m^2/s) implying the major contribution of structure diffusion to the proton conduction in presence of an acid [9]. The results obtained in the study are in close analogy to that reported by Goward et al. on the basis of solid state NMR [47]. The mobile NH protons involved in weak hydrogen bonds were found to contribute significantly to structure diffusion than the rigid ones. Schuster et al. proposed structure diffusion as dominant conduction mechanism in immobilized heterocycles [8]. The proton migration was found to occur within the crystal aggregates formed by imidazole units through hydrogen bonding interaction.

4. Conclusions

This study investigated the influence of crystal morphology of 1*H*-1,2,4-triazole (Taz) as a solid proton solvent dispersed in sulfonated polyetherimide (SPEI) matrix on anhydrous state proton conductivity of the polyelectrolytes. Bisphenol A polyetherimide was sulfonated to three different degrees (22, 48 and 62%) by trimethylsilylchlorosulfonate (TMSCS) and novel anhydrous proton conducting polyelectrolytes were prepared by incorporation of 1*H*-1,2,4-triazole (Taz) in SPEI matrix. FT-IR spectroscopy and DSC study revealed specific interactions between sulfonic acid groups and triazole molecules. The intermolecular interactions and their effect on size, shape and state of dispersion of triazole crystals were analyzed as a function of degree of sulfonation and triazole concentration. The sulfonic acid groups provided strong binding sites and induced nucleation of triazole. WAXD and AFM analysis showed gradual reduction of crystal size and their uniform distribution throughout the sulfonated polymer matrix with increasing concentration of the sulfonic acid. The decrease in size caused melting point depression and thus the molecular mobility in smaller size crystals improved below the melting temperature of

pure triazole. Within each crystal domain, two different states of triazole molecules were evident due to the different degrees of association with sulfonic acid groups; strongly bound and weakly bound/self-associated free triazole. Intermolecular proton transfer in the crystal domain occurred through the hydrogen bonded structure formed by these triazole molecules (structure diffusion).

References

[1] Kreuer KD. J Membr Sci 2001;185:29.
[2] Mauritz KA, Moore RB. Chem Rev 2004;104:4535.
[3] Hickner MA, Ghassemi H, Kim YS, Einsla BR, McGrath JE. Chem Rev 2004; 104:4587.
[4] Dippel T, Kreuer KD, Lassegues JC, Rodriguez D. Solid State Ionics 1993;61:41.
[5] Wainright JS, Wang J-T, Savinell RF, Litt M, Rogers MC. Proc Electrochem Soc 1994;94:255.
[6] Bozkurt A, Ise M, Kreuer KD, Meyer WH, Wegner G. Solid State Ionics 1999;125:225.
[7] Kreuer KD, Fuchs A, Ise M, Spaeth M, Maier J. Electrochim Acta 1998;43:1281.
[8] Schuster MFH, Meyer WH, Schuster M, Kreuer KD. Chem Mater 2004;16:329.
[9] Li S, Zhou Z, Zhang Y, Liu M. Chem Mater 2005;17:5884.
[10] Zhou Z, Li S, Zhang Y, Liu M, Li W. J Am Chem Soc 2005;127:10824.
[11] Genies C, Mercier R, Sillion B, Cornet N, Gebel G, Pineri M. Polymer 2001; 42:359.
[12] Lee C, Sundar S, Kwon J, Han H. J Polym Sci Part A Polym Chem 2004;42:3612.
[13] Lee C, Sundar S, Kwon J, Han H. J Polym Sci Part A Polym Chem 2004;42:3621.
[14] Fang J, Guo X, Harada S, Watari T, Tanaka K, Kita H, et al. Macromolecules 2002;35:90224.
[15] Yin Y, Suto Y, Sakabe T, Chen S, Hayashi S, Mishima T, et al. Macromolecules 2006;39:1189.
[16] Kerres J, Ullrich A, Hein M, Gogel V, Friedrich KA, Jörissen L. Fuel Cells 2004;4:105.
[17] Kerres JA. Fuel Cells 2005;5:230.
[18] Kerres JA, Ullrich A, Meier F, Häring T. Solid State Ionics 1999;125:243.
[19] Kerres JA. J Membr Sci 2001;185:3.
[20] Deimede V, Voyiatzis GA, Kallitsis JK, Qingfeng L, Bjerrum NJ. Macromolecules 2000;33:7609.
[21] Kim YS, Dong L, Hickner MA, Glass TE, Webb V, McGrath JE. Macromolecules 2003;36:6281.
[22] Laporta M, Pegoraro M, Zanderighi L. Phys Chem Chem Phys 1999;1:4619.
[23] Kim YS, Dong L, Hickner MA, Pivovar BS, McGrath JE. Polymer 2003; 44:5729.
[24] James PJ, Elliott JA, McMaster TJ, Newton JM, Elliott AMS, Hanna S, et al. J Mater Sci 2000;35:5111.
[25] Park H, Kim Y, Hong WH, Choi YS, Lee HK. Macromolecules 2005;38:2289.
[26] Guan R, Dai H, Li C, Liu J, Xu J. J Membr Sci 2006;277:148.
[27] Tsatsas AT, Risen WM. J Polym Sci Part B Polym Phys 1993;31:1223.
[28] Alberti G, Casciola M, Massinelli L, Bauer B. J Membr Sci 2001;185:73.
[29] Gebel G. Polymer 2000;41:5829.
[30] Kreuer KD, Paddison SJ, Spohr E, Schuster M, Meyer WH, Schuster M. Chem Rev 2004;104:4637.
[31] Kreuer KD. Solid State Ionics 2000;136–137:149.
[32] Kim J-D, Mori T, Hayashi S, Honma I. J Electrochem Soc 2007;154:A290.
[33] Gunday ST, Bozkurt A, Meyer WH, Wegner G. J Polym Sci Part B Polym Phys 2006;44:3315.
[34] Guhathakurta S, Min K. PMSE Preprints 2008;98:849–50.
[35] Guhathakurta S, Min K. J Polym Sci Part B Polym Phys, submitted for publication.
[36] Chowdhury A, Thynell ST. Thermochim Acta 2007;466:1.
[37] El-Azhary AA, Suter HU, Kubelka J. J Phys Chem A 1998;1998:102.
[38] Krishnakumar V, Xavier RJ. Spectrochim Acta Part A 2004;60:709.
[39] Colthup NB, Daly LH, Wiberley SE, editors. Introduction to infrared and Raman spectroscopy. New York: Academic Press; 1990.
[40] Goldstein P, Ladell J, Abowitz G. Acta Crystallogr B 1969;25:135.
[41] Adams GW, Cowie JMG. Polymer 1996;40:1993.
[42] Fielding L. Tetrahedron 2000;56:6151.
[43] Burckhalter JH, Campbell JR. J Org Chem 1961;26:4232.
[44] Deuschl H. Ber Bunsen-Ges Phys Chem Ber 1965;69:550.
[45] Cullity BD. Elements of X-ray diffraction. Reading, Mass: Addison–Wesley; 1978. p. 281–323 [chapter 9].
[46] Lin J, Cates E, Bianconi PA. J Am Chem Soc 1994;116:4738.
[47] Goward GR, Schuster MFH, Sebastiani D, Schnell I, Spiess HW. J Phys Chem B 2002;106:9322.